University of BRISTOL

Department Of Physics

# FINAL YEAR PROJECT, DISSERTATION OR PHYSICS EDUCATION REPORT

| | |
|---|---|
| NAME: | Luka Milic |
| DEGREE COURSE: | Mathematics and Physics (MSci) |
| PROJECT TITLE: | Entanglement of photons pairs generated in silicon ring resonators |
| YEAR OF SUBMISSION: | 2015 |
| SUPERVISOR: | Damien Bonneau, Josh Silverstone and Mark Thompson |
| NUMBER OF WORDS: | 4000 (exclude appendices, references, captions and abstract) |

# Entanglement of photons pairs generated in silicon ring resonators

Luka Milic

April 24, 2015

**Abstract**

Do the abstract last.

**Acknowledgements**

Thank you Damien and Josh for your invaluable help throughout my project. Lizzy for working with me in the lab. Imad for your help and encouragement. Mark for giving me the opportunity and supervision. Raf for your help and Phil for supplying sarcasm.

# Contents

# 1 Introduction

The endeavour to build a quantum computer holds the promise of solving computational problems which are currently intractable on classical computers. A particularly promising paradigm for this is the linear optical quantum computer (LOQC) model which in theory allows for scalable universal quantum computation. Work on LOQC can be done using bulk optics components but this quickly becomes impractical when the experiments need to be scaled up to more qubits. Integrated photonics is a solution to this problem and allows for experiments with a much higher component density, an essential ingredient to scalable quantum computing. Many components from bulk optics have equivalents on these photonic chips with popular materials being silicon-on-insulator (SOI) , lithium niobate and glass materials. Here we focus on SOI chips as they have many promising properties for the implementation of complex quantum optical circuits.

A key requirement for the full implementation of LOQC is a scalable, bright, deterministic and indistinguishable single photon source. Single photon sources in the SOI platform are typically made from the waveguide itself and use the spontaneous four-wave mixing which occurs in silicon due to the third order non-linearity to create a single photon pair. This report aims to develop a method of measuring the indistinguishably of the produced photons with a classical technique, exploiting stimulated four-wave mixing. This method collects a joint spectrum which is an estimation of the spectral shape of the two photons produced by the source. For a full description, the Joint Spectral Amplitude JSA is the desired quantity and this is a full description of the wavefunction of the single photons emitted by the silicon ring resonators. However it is only within the scope of this work to measure the Joint Spectral Intensity, which is the absolute value squared of the JSA. This gives an estimate of the JSA and allows the purity to be bounded from above.

The mission is therefore to develop a methodology to reconstruct these wavefunctions and hence engineer indistinguishable (high purity) single photon sources. In this work we performed such measurements on three SOI chips. The experimental work started with an initial proof of concept that one can collect joint spectrum data in the way desired. This was done on a chip supplied by Marc Sorel from Glassgow University. Then due to the fragility of these chip at high powers the experiment progressed to a chip manufactured by Toshiba. Finally in order to investigate a promising new material, amorphous silicon chip was used for experiments.

In parallel techniques of analysing the output data are developed. Filtering techniques which remove noise are developed in order to extract the relevant signals. A general framework is set out which aims to quantify the certainty in the measurements.

Finally we conclude that there is still much to be done in this area, proposing an outline for how to carry out effective measurements in the future.

# 2 Detailed Background and Theory

## 2.1 From Feynman to the linear optical quantum computer

It was Richard Feynman in 1982 [1] who first imagined it might be possible to efficiently simulate quantum systems with other quantum systems and hence end up doing computations that no classical computer can do in a reasonable (polynomial) time. The basic element of a quantum computer is the qubit, which can be written as

$$|\psi\rangle = \alpha\,|0\rangle + \beta\,|1\rangle \tag{2.1}$$

this says the qubit is in a superposition of being in the $|0\rangle$ and $|1\rangle$ state at the same time, where $\alpha$ and $\beta$ are the complex probability amplitudes. If we perform a measurement there is a $|\alpha|^2$ probability of measuring $|0\rangle$ and a $1 - |\alpha|^2 = |\beta|^2$ probability of measuring $|1\rangle$. This is a generalization of the classical bit, which can only ever be set to 0 or 1. With this added structure, quantum computers can in theory out perform classical computers in certain tasks such as factorisation [2], meteorology [3], quantum chemistry [4] and they can be used to establish communication systems secured by the laws of physics with quantum key distribution (QKD) [5].

With the exception of QKD none of these applications have yet been fully realised, in particular because not all of the criteria [6] set out in 1998 by DiVincenzo for a universal quantum computer have been met. These are:

- A scalable physical system with well characterized qubits
- The ability to initialize the state of the qubits to a simple fiducial state, such as $|000...\rangle$
- Long relevant decoherence times, much longer than the gate operation time
- A universal set of quantum gates
- A qubit-specific measurement capability

This work aims to make some progress on the first two criteria in the context of integrated optical quantum computers. Here we define qubits as photons, with $|0\rangle$ and $|1\rangle$ denoting the path a photon takes through a linear optical quantum circuit (LOQC). Figure 2.1 shows how a LOQC fits into a wider context, with single photon sources supplying qubits, single photon detectors reading out the results of the computations and a classical computer which reconfigures the circuit using the detection results. We now discuss what kind of single photon source would satisfy these criteria.

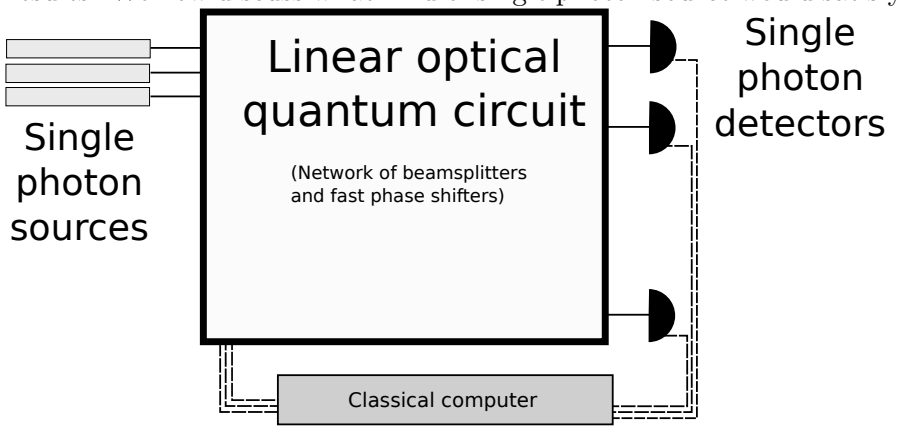

**Figure 2.1:** A conceptual outline of the architecture of a optical quantum computer, single photon sources supply the qubits which are fed into reconfigurable circuits which are altered depending on the pattern of photons detected at the detectors.

## 2.2 Generating single photons

The ideal single photon source would produce exactly one photon when triggered in a pure quantum state, where pure means it is in a state superposition of all of its spectral components rather than a statistical mixture. This happens if the temporal shape is the same as the Fourier transform of its spectrum [7]. Such a perfect source does not yet exist. We can divide existing sources into two categories, deterministic and probabilistic [8]. The first kind are typically small single atom or molecule systems, which respond deterministically to some kind of impulse. For example a single atom two level system can be excited by a laser pulse into the upper level, it will then emit a photon of some fixed energy after some relaxation time. Non-deterministic or probabilistic sources on the other hand must be heralded so that there is knowledge of when they fired.

In the past these experiments have typically been performed with bulk optics meaning that each element is fixed to a large optical work bench, carefully aligned with the next element and with the light travelling in the air in between. These experiments take up a lot of lab space and quickly encounter resource constraints if they try to become too complex. A solution to this is to translate each of the components onto a integrated chip, where far less alignment is needed, the important devices always maintain the same separation and most importantly vastly more complicated circuits can be designed. This is of course essential to the endeavour of using LOQC's to perform complex quantum operations. Note again Divencenzo's first criteria, referring to scalability, integrating photonics onto chips makes a lot of progress on this front.

Photonics can be integrated onto chips of various materials, typical choices are glass, lithium niobate and silicon. Here we focus on silicon, it has the advantage that advanced fabrication techniques exist due to the multi-billion dollar semiconductor industry. Two types of silicon are used, the first is the standard silicon with its periodic lattice structure and the second is amorphous silcion which forms a random network structure. Amorphous silicon could potentially solve problems with standard silicon such as two photon absorption and subsequent free carrier absorption which is known to be detrimental to single photon sources.

On chip single photon sources on silicon have been studied [9, 10] and shown to be a promising platform. Currently two ways of producing photons are employed. The first way employs large spools of waveguide (to increase photon production probability) towards the start of the circuit into which a intense laser beam (referred to as the pump) is injected and due to non-linear processes single photons are produced. This happens because silicon has a $\chi^{(3)}$ non-linearity and so a small amount of frequency conversion occurs. The process called spontaneous four wave mixing (SFWM) takes two pump photons $\omega_{p_1}$, $\omega_{p_2}$ and converts them into a signal $\omega_s$ and $\omega_i$ idler according to the following energy conservation equation.

$$\omega_{p_1} + \omega_{p_2} = \omega_s + \omega_i \tag{2.2}$$

This equation works in general, for a laser beam with only one frequency we write $2\omega_p = \omega_s + \omega_i$. An upshot of producing two photons is that this is a heralded single photon source, meaning it is possible to know when you've generated a photon by using, for example, the idler as your herald and the signal as the heralded photon.

A second alternative way to control the generation of the single photons is to create a cavity into which the beam can couple and produce single photon pairs (signal and idlers) with a higher probability. The cavity which we focus on is the ring resonator, a structure with interesting spectral properties which can be manipulated to increase the purity of the generated photons.

### 2.3 Four wave mixing in silicon waveguides

Here we motivate some of the theoretical background to four wave mixing in order to arrive at why ring resonators can be used to better exploit the process.

Waves travel through non-linear materials according to the non-linear wave equation:

$$\nabla^2\mathbf{E} - \frac{n^2}{c^2}\frac{\partial^2}{\partial t^2}\mathbf{E} = \frac{1}{\varepsilon_0 c^2}\frac{\partial^2}{\partial t^2}\mathbf{P}^{NL} \tag{2.3}$$

$$\mathbf{P}^{NL} = \sum_{n=0}^{\infty} \epsilon_0 \chi^{(n)} \mathbf{E}^n(\mathbf{x}, t) \tag{2.4}$$

Where $\mathbf{P}^{NL}$ accounts for the non-linear response of the material and $\mathbf{E}(\mathbf{x}, t)$ is the electric field . In silicon the predominant non-linear effect comes from the $\chi^{(3)}$ term, as this is a third order term, it enables wave mixing processes, a quick intuition for this can be gained by inputting into $\epsilon_0\chi^{(3)}\mathbf{E}^3(t)$ a super position of two waves:

$$\mathbf{E}(t) = E_s\cos(\omega_s t) + E_p\cos(\omega_p t) \tag{2.5}$$

The result is proportional to:

$$E_p E_s^2\cos((2\omega_s - \omega_p)t) + E_p E_s^2\cos((2\omega_s + \omega_p)t) \tag{2.6}$$

$$+ E_p^2 E_s\cos((2\omega_p - \omega_s)t) + E_p^2 E_s\cos((\omega_s + 2\omega_p)t) + h.t. \tag{2.7}$$

Where $h.t.$ are the harmonic terms, such as $E_1^3\cos(3\omega_p t)$ which are we aren't interested in here. We notice that four new frequencies are generated, in experiments one typically denotes $E_p$ the pump and $E_s$ the signal, with $E_p >> E_s$. Due to the pump beam being of higher intensity we are left with two dominant processes:

$$2\omega_p + \omega_s = \omega_i^{(1)} \tag{2.8}$$

$$2\omega_p - \omega_s = \omega_i^{(2)} \tag{2.9}$$

We call the resulting beam $\omega_i$ the idler. Now we take interest in the second process(equation 2.9) because this is one typically used in quantum optics to produce photon pairs for a single photon sources and it has better phase matching conditions. Rewriting it as $2\omega_p = \omega_i + \omega_s$ and thinking of the classical waves as streams of photons we can see that two pump photons can be converted into signal and idler photons. This conversion is allowed due to vacuum fluctuations stimulating the process, these are very weak and so the efficiency of the process is also quite low.

Discussion of phase matching has been omitted, but it is enough to say that in order for the process to constructively interfere and hence satisfy the wave equations we must have $2\mathbf{k_p} = \mathbf{k_i} + \mathbf{k_s}$.

Now in order to take this process to the single photon level we must introduce a way to talk about photons at the quantum scale. Because of the Heisenberg uncertainty principle the number of photons at each energy level can be uncertain. Such states are described by a vector in fock

space, for example a state where there are two photons in the first and third energy level would be written as:

$$|2020...\rangle \tag{2.10}$$

The state for the vacuum or in other words for no photons is written as:

$$|vac\rangle = |000...\rangle \tag{2.11}$$

Operators exist to create and annihilate photons.

$$a_i^\dagger |n_1, ..., n_i, ...\rangle = \sqrt{n_i + 1} |n_1, ..., n_i + 1, ...\rangle \tag{2.12}$$
$$a_i |n_1, ..., n_i, ...\rangle = \sqrt{n_i} |n_1, ..., n_i - 1, ...\rangle \tag{2.13}$$
$$\tag{2.14}$$

With commutation relations $[a_i, a_j] = [a_i^\dagger, a_j^\dagger] = 0$ and $[a_i, a_j^\dagger] = \delta_{ij}$

The non-linear hamiltonian that governs the spontaneous four wave mixing process in the waveguide is:

$$\hat{H}_{NL} = -\chi^{(3)} \int_\infty^\infty \int_\infty^\infty \int_\infty^\infty \int_\infty^\infty S(k_{p_s}, k_{p_i}, k_{p_1}, k_{p_2})(a_{k_{p_i}}^\dagger a_{k_s}^\dagger a_{k_{p_1}} a_{k_{p_2}} + h.c.) dk_{p_s} dk_{p_i} dk_{p_1} dk_{p_2} \tag{2.15}$$

The linear vacuum hamiltonian is also involved:

$$\hat{H}_L = \int_\infty^\infty a_k^\dagger a_k dk \tag{2.16}$$

Adding these two up gives the overall hamiltonian $\hat{H} = \hat{H}_L + \hat{H}_{NL}$. The function $S(k_{p_s}, k_{p_i}, k_{p_1}, k_{p_2})$ represents the coupling between the various frequencies.

This general frame work applies to both straight waveguide and ring resonator production of photon pairs. There is a large amount of literature [,,,,] which describes how to use it to derive the resultant wavefunction, here we simply state the general result:

$$|\psi_{out}\rangle = \left[1 + \frac{\beta}{\sqrt{2}} \int dk_1 dk_2 \Phi(k_1, k_2) a_{k_1}^\dagger a_{k_2}^\dagger\right] |vac\rangle \tag{2.17}$$

This is called the biphoton wavefunction, the reason we omit the full theory is because this project focuses on measurement and analysis of $\Phi$ rather than it's exact theoretical origin. The biphoton wavefunction encodes all of the information about how the photon pairs were produced that effect its spectral and phase distribution. This includes the pump spectrum, intensity, the geometry of the waveguide or cavity used for the process.

This biphoton wavefunction can be produced by injecting a laser into the waveguide and so supplying two pump photons. Furthermore with the classical motivation in mind, this process can be stimulated by adding a further laser at the idler or signal frequency. This allows for the measurement of $\Phi$ in slices using an optical spectrum analyser. The theory of this is described in section 2.7.

This function $\Phi(k_1, k_2)$ is called the joint spectral amplitude (JSA) and its absolute value squared is called the joint spectral intensity (JSI). Returning to DiVenceno's criteria we require

that this function is of the form $\Phi(k_1, k_2) = f(k_1)g(k_2)$ to explain this we introduce some more quantum theory.

A two party system in quantum mechanics can be described generally as:

$$|\psi\rangle = \sum_{i,j} \alpha(i,j) \, |i\rangle_A \otimes |j\rangle_B \tag{2.18}$$

This state can be a pure state, so that $\alpha(i,j) = f(i)g(j)$ and so

$$|\psi\rangle = \left( \sum_i f(i) \, |i\rangle_A \right) \otimes \left( \sum_j g(j) \, |j\rangle_B \right) \tag{2.19}$$

meaning that there is no way that a measurement which happens in system A can effect system B. Otherwise it is in an entangled state and the sub systems act as statistical mixtures. The same idea can be applied to the wavefunction in equation 2.17 to give:

$$|\psi_{out}\rangle = \left[ 1 + \frac{\beta}{\sqrt{2}} \int dk_1 f(k_1) a^\dagger_{k_1} \int dk_2 f(k_2) a^\dagger_{k_2} \right] |vac\rangle \tag{2.20}$$

Which now says, if you measure the first photon there is no way you can influence the second photon. For a heralded source this is vital, the process of heralding must not interfere with the heralded photon and in particular not in this way as here it would make the photon collapse randomly into one of its modes.

In order to talk about how pure or mixed a biphoton wavefunction, the JSA can be decomposed into a linear superposition of pure states. This is written as [11]:

$$\Phi(k_1, k_2) = \sum_i \lambda_i f_i(k_1) g_i(k_2) \tag{2.21}$$

With $\sum_i \lambda_i = 1$. Now it is possible to assess the separability of such a JSA by choosing a metric to quantify how many terms equation 2.28 has. A convenient one is the purity defined as:

$$P = \sum_i \lambda_i^4 \tag{2.22}$$

For a totally separable state where there is only one $\lambda$ coefficient, $P = 1$ and this is the maximum purity of any system. The minimum value of P is less well defined and depends on the dimension of the system but for systems with large dimensionality the minimum approaches zero, in particular for spaces like frequency which have a infinite dimension the minimum is zero.

## 2.4 Analysis of the JSI

Assuming we have collected a JSI ($|\Phi(k_1, k_2)|^2$) we now want to find out how we can extract the most information possible about the separability of the state $|\psi_{out}\rangle$. Due to finite precision on the experimental apparatus the JSI will be discretised and also cropped into some frequency region. Furthermore noise will be introduced into the measurement and we make the approximation that $\sqrt{|\Phi(k_1, k_2)|^2} \sim \Phi(k_1, k_2)$ which is analogous to discarding the phase information. The discretisation and cropping of the JSI can be expressed as

$$\sum_{\omega_1,\omega_2} \Phi(\omega_1,\omega_2)|\omega_1\rangle\langle\omega_2| \tag{2.23}$$

where we sum over some finite region with finite increments. Also there will be some experimental noise, we can illustrate this be adding a matrix of random numbers on the order of the experimental noise:

$$\mathbf{f} = \sum_{\omega_1,\omega_2} \Phi(\omega_1,\omega_2)|\omega_1\rangle\langle\omega_2| + \mathbf{n} \tag{2.24}$$

Now to approximate the purity we use the formula:

$$P = \frac{1}{K} \approx \frac{\mathrm{Tr}\left[(\mathbf{f}^\dagger\mathbf{f})^2\right]}{\mathrm{Tr}\left[\mathbf{f}^\dagger\mathbf{f}\right]^2} \tag{2.25}$$

Where P is the purity and K is the schmidt number. The schmidt number is an indication of how many modes are required to construct the wavefunction as in equation 2.28. A full derivation of this is in appendix A. Appendix A.2.2 proves also that this process is equivalent to quantifying the number of terms required in an SVD decomposition and so a further expression is derived:

$$\frac{\mathrm{Tr}\left[(\mathbf{f}^\dagger\mathbf{f})^2\right]}{\mathrm{Tr}\left[\mathbf{f}^\dagger\mathbf{f}\right]^2} = \frac{\sum_i \lambda_i^4}{\left(\sum_j \lambda_j^2\right)^2} \tag{2.26}$$

Where $\lambda_i$ are the singular values of the matrix $\mathbf{f}$. The SVD decomposition of $\mathbf{f}$ is:

$$\mathbf{f} = \sum_i |u_i\rangle\, \lambda_i\, \langle v_i| \tag{2.27}$$

This has the same form as

$$\Phi(k_1,k_2) = \sum_i \lambda_i f_i(k_1) g_i(k_2) \tag{2.28}$$

and this is called the schmidt decomposition. So by using the purity formula (equation 2.25) on $\mathbf{f}$ we have found a way to estimate the number of modes in our bi-photon wave function, which is the quantity we want to minimise for an ideal single photon source.

### 2.4.1 Purity formula examples

In this section we probe the behaviour of the purity formula (equation 2.25) which was found in the previous section. The main aim is to numerically simulate how experimental error effects the calculated purity. This is achieved by plotting the four characteristic functions as in figure 2.2. Function a) illustrates that a flat function is completely separable, this obvious result will be important later on when considering how cropping effects the JSI. Function b) comes from the simulation of a ring resonator (see section 2.5) biphoton wavefunction. Function c) is simply a straight line an example of a function which is not very seperable. Function d) is similar, but with a gaussian cross section, this is included to mirror what happens in a straight waveguide source.

Although a straight waveguide source will have a different shape, the response to noise should be similar. This claim is backed up by the fact that a) and b) respond similarly to the addition of noise.

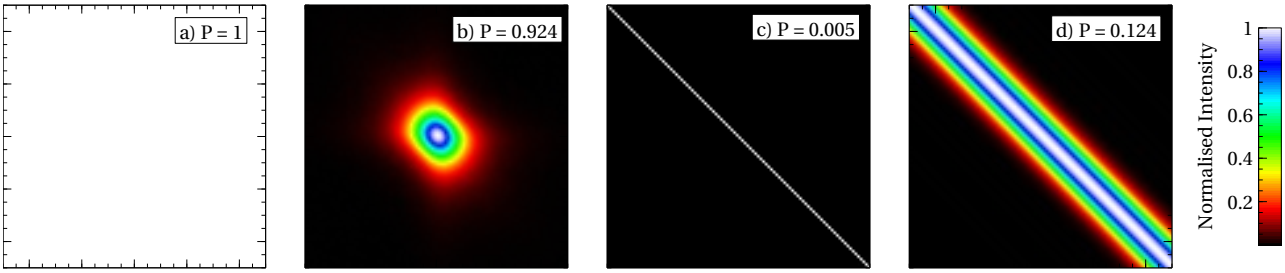


**Figure 2.2:** Four illustrative functions with purtiies calculated **a)** A constant function $f(x, y) = 1$ **b)** A simulation of a biphoton wavefunction from a ring resonator **c)** A straight line, 1 pixel wide, $f(x, y) = \delta(x-y)$ **d)** A straight line with gaussian crosssection $f(x, y) = e^{-(x-y)^2}$. Each plot is a 200 by 200 floating point array.

By slowly adding more noise to these four functions the plots in figure 2.2 are obtained. Figure 2.4 shows the functions after all the noise has been added. It is at first obvious that they have all converged to nearly the same purity of roughly $0.8 \pm 0.5$ which is independent of dimension for plots bigger than 10 by 10 pixels (for smaller dimensions the purity is erratic and of a higher value due to the numbers being random and sometimes forming shapes which are even more separable). It is somewhat unfortunate that random noise has such impact on measurements, in particular looking at the functions after noise has been added their original structures are still visible but the purity value is completely wrong. However with the SNR graph we can at least quickly develop a way to calculate the error in experimental data.

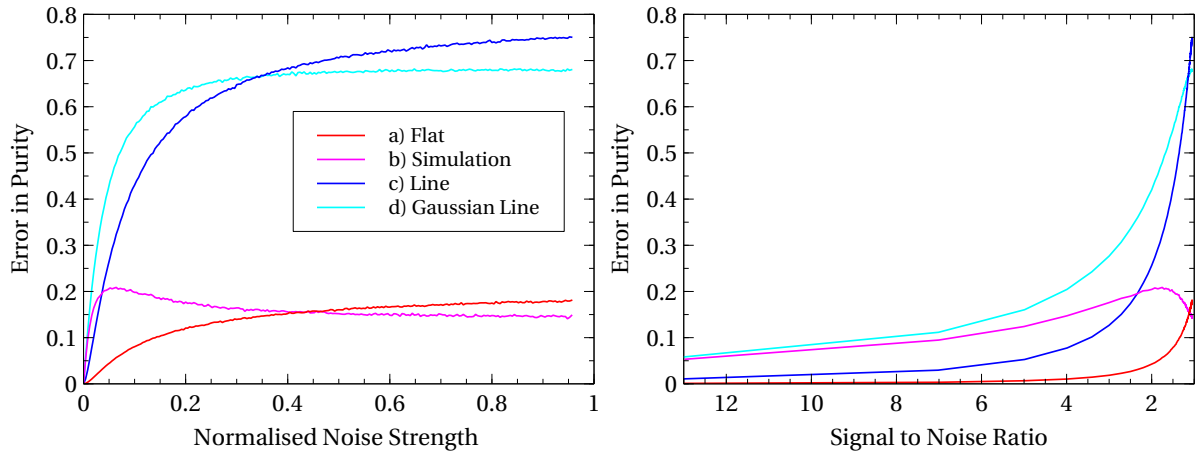


**Figure 2.3:** Two graphs showing how the error in the purity calculation for functions **a,b,c,d** changes with the addition of noise. They differ only by the x-axis, the noise is guassion noise, the SNR is calculated by dividing the amount of original function by the amount of added noise.

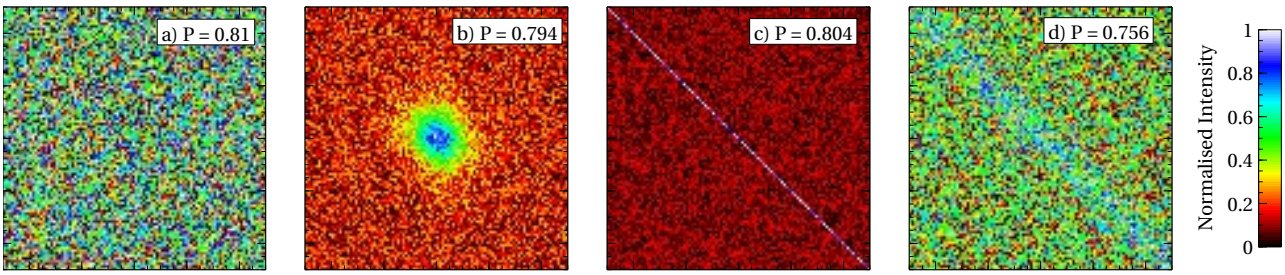


**Figure 2.4:** The functions a,b,c,d from figure 2.2 after the most noise has been added, intermediate changes in the purity are shown in 2.3

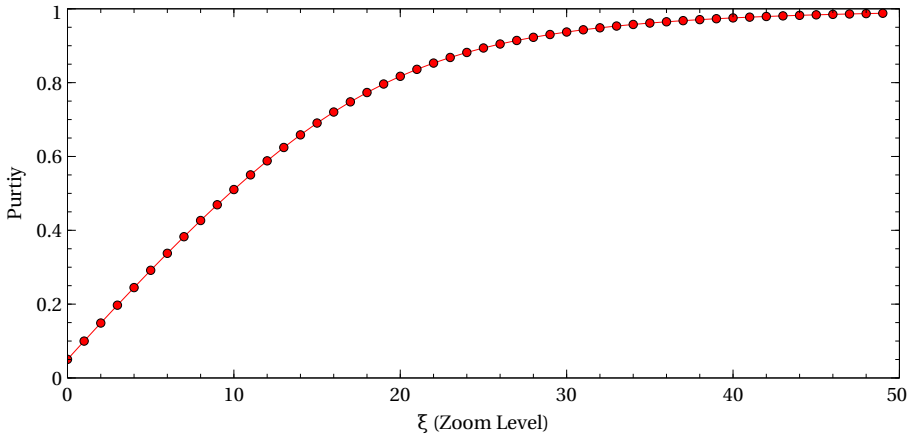


**Figure 2.5:** A plot of purities for the function $f(x, y) = e^{-(x+y)^2/\xi^2}$ at varying $\xi$ values. This acts in the same way as zooming or cropping a JSI would. A clear trend of increasing purity is observed. This data was obtained with the function plotted on a 50 by 50 array.

Figure 2.5 shows that zooming into a JSI function always increases the purity, this is because the function becomes more and more flat as you zoom in. This point is relevant in the context of engineering JSI, it means that by using filters the purity can be increased. However more filters introduces more loss and so an optimum point must be found.

For trying to get a highly accurate value for the purity of some biphoton wavefunction the implication is that.

## 2.5 Ring Resonators

Using ring resonators as a way to improve the separability of the JSA has been tried and found to work. Here we describe why it works and the general workings of a ring resonator, we then finally move onto discussing metrics to quantify this separability in terms of purity and schmidt number.

Ring resonators are one of many devices which can be found on optical circuits on chip. They are closed strips of waveguide, placed near enough to the waveguide carrying light so that light can evanescently couple inside, in other words they form a cavity. By setting up a simple experiment, where light passes by the resonator and the transmission is measured for varying wavelengths a spectrum characterising the ring can be obtained. An example of one is shown in figure 2.6, periodic resonances are visible with a spacing called the free spectral range (FSR). The physical reason for the resonances is that when the input beam is an integer number of wavelengths of the

circumference of the ring, a high amount of destructive interference occurs because the light picks up a $\pi$ phase shift from coupling across waveguides.

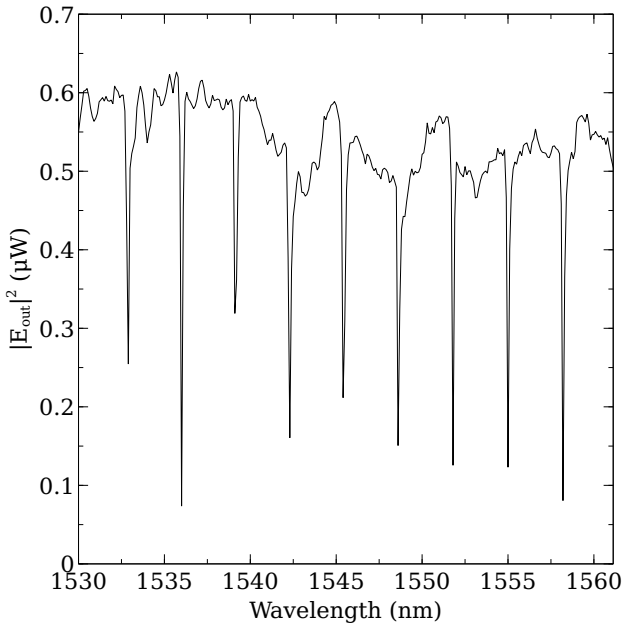


**Figure 2.6:** A typical ring resonator spectrum.

A first order model for a ring resonator is called the linear ring model, this does not include non-linear effects which are discussed later but does allow for a good understanding of the different coupling modes a ring can be in. Following figure 2.5 $E_{in}$ is the injected laser beam and $E_{out}$ is the output light, where $|E_{out}|^2$ is what is typically measured in an experiment. $E_1$ is the field at the start of the ring and $E_2$ is the field at the end of the ring, by travelling around the ring some of the light is lost and a wavelength dependant phase relative to the input light is picked up.

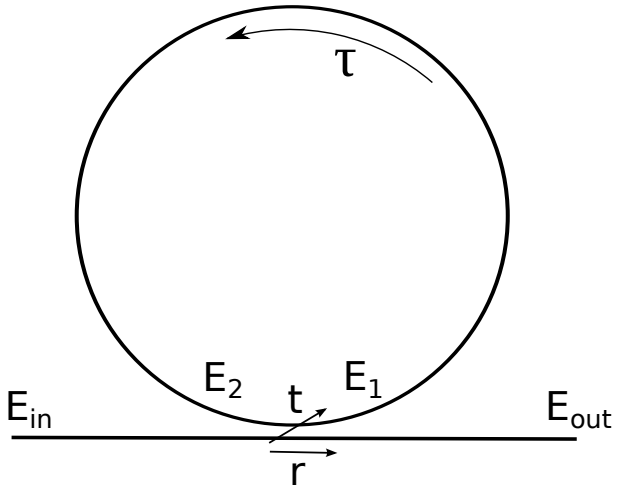

**Figure 2.7:** A simple but powerful model of a ring resonator. $E_{in}$ represents the input electrical field and $E_{out}$ is the field after interaction with the ring. $E_1$ is the field at the start of the ring and $E_2$ is this field with some loss due to propagation through the ring waveguide. We assume that the distance between $E_{out}$ and $E_{in}$ is much smaller than $E_1$ and $E_2$.

We can model this system with the following set of linear equations, where $r$ is the fraction of light that passes by the coupling region and $t$ is the amount of light that couples across the coupler.

$$\begin{pmatrix} E_{out} \\ E_1 \end{pmatrix} = \begin{pmatrix} r & it \\ it & r \end{pmatrix} \begin{pmatrix} E_{in} \\ E_2 \end{pmatrix} \tag{2.29}$$

With these matrices and also by noting that $E_2 = \tau e^{i\theta} E_1$ is due to the ring causing a phase difference and some loss. We can derive expressions for each point in the system, for the full derivation refer to appendix C.

$$\left|\frac{E_{out}}{E_0}\right|^2 = \frac{r^2 - 2r\tau\cos(\theta) + \tau^2}{1 + r^2\tau^2 - 2r\tau cos(\theta)} \tag{2.30}$$

$$\left|\frac{E_1}{E_0}\right|^2 = \frac{1 - r^2}{1 + r^2\tau^2 - 2r\tau cos(\theta)} \tag{2.31}$$

$$\left|\frac{E_2}{E_0}\right|^2 = \tau^2 \left|\frac{E_1}{E_0}\right|^2 \tag{2.32}$$

Where $\theta = kL = \frac{2\pi n_{eff}}{\lambda} L$. The analysis also finds the relation $r^2 = 1 - t^2$ , which is useful because it reduces the amount of variables we need to model the resonator.

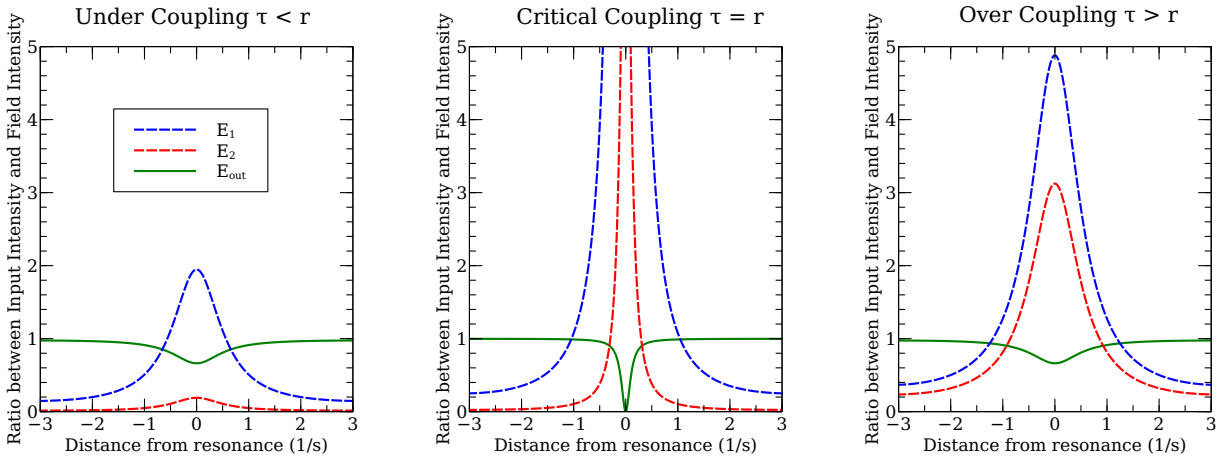


**Figure 2.8:** Notice how similar under and over coupling are to each other

Figure 2.8 shows the 3 main regimes that can be achieved by varying $r$ and $\tau$. The first is under-coupling, a typically undesirable set up where the ring loses more light than it recieves and hence performs low quality filtering. This looks identical to over-coupling where more light enters then ring than is lost. The fact that over and coupling look the same is an important point for later analysis, as when using a resonator as a single photon source, a small amount of over-coupling is desirable.

Critical coupling occurs when the loss within the ring is balanced with the amount of light coupling in ($r = \tau$) this gives a spectrum with the highest quaility factory, where we define quality factor[REF] as:

$$Q \approx \frac{2\pi L n_{eff}}{-\lambda \ln r\tau} \tag{2.33}$$

This metric is useful for comparing rings.

## 2.6 Bistability

It can be experimentally observed that injecting power into a ring resonator will cause changes in the spectral position and shape of the resonance. Typically in silicon ring resonators the more power in the ring the more the resonance position is red-shifted by the thermo-optic effect [12]. A counter acting effect is carrier generation induced by two-photon absorption [13] which causes a blue-shift in the resonance position. This carrier generation process is much faster than the thermo-optic process so it more relevant to lasers with low repetition rates.

The bistability effect is observed by changing the power injected into the ring resonator at a fixed wavelength. By steadily increasing the power of a monochromatic light source injected into the ring at a wavelength slightly higher than the resonance position $\lambda_r$ of the ring, $\lambda_r$ is increased (thermal effects dominate as the laser is a continuous wave and not pulsed). The shift in $\lambda_r$ accelerates as more light is coupled into the ring and transmission falls as more light is coupled into the ring. The system is now in a different and stable state (assuming the injected light is not discontinued). With a low intensity probe it is now possible to map out the new position and shape of the resonance.

By doing the reverse experiment with the input power decreasing a similar phenomena is observed, however the sudden accelerating changing in resonance position is seen for a different power due to the ring coming from a different stable state. A hysteresis loop can be observed.

Some knowledge of this effect is vital when planning experiments using high and variable powers, as one must take into account that the state of the ring is not fixed. Furthermore when automating equipment it may be vital to integrate knowledge of this into any scanning procedures.

## 2.7 Characterisation of quantum processes with classical techniques

The theory to support this quantum measurement with classical techinques has been developed [14] and it turns out the quantum and classical processes are direct analogues to each other. The ratio between their powers follows a simple formula:

$$\frac{P_{i,Q}}{P_{i,C}} = \frac{1}{4Q}\frac{\hbar\omega_p^2}{P_s} \tag{2.34}$$

Where $P_s$ is the input power of the seed laser used to amplify the quantum process and $\omega_p$ is the frequency of the laser which pumps the ring resonator and $Q$ is the quality of the ring (defined in section 2.5).

### 2.8 Alternative methods of finding the purity

### 2.9 What experiments can be done?

# 3 Method

Here the methodology and equipment choices of the performed experiments are described. The logical place to begin is with the silicon chips, which are the central object of interest in the experiments. The chips used were had a typical area of $1\,\mathrm{cm}^2$ and a thickness of a few millimetres. In order to couple light into the waveguides etched onto the chip spot size converters or diffraction gratings are used. For spot size converters figure 2.8 shows the procedure. The fibre which directs the light is called a lense fiber, it has a focal point a few micrometers in front of its tip, allowing high accuracy coupling onto the converters. For this type of coupling peizometers were used with a recoupling algorithm.

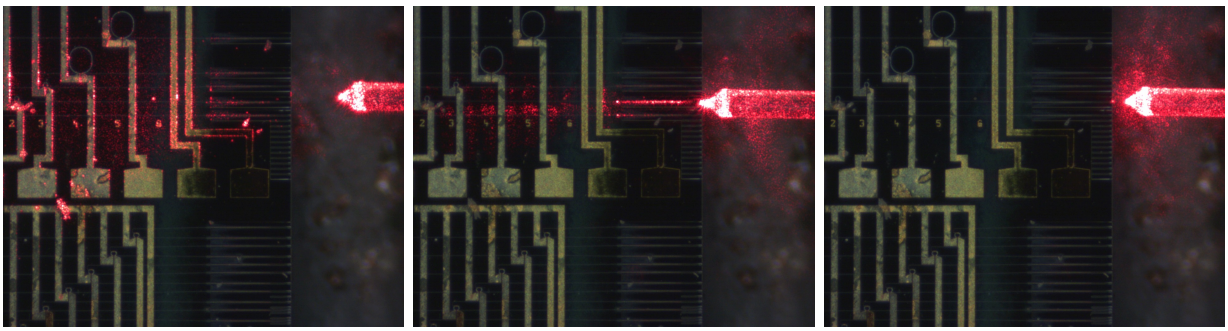

**Figure 3.1:** The first image shows the lense fiber above the chip, illuminating its surface, then the fiber has found a good coupling position and finally it is too far underneath the chip. Red light is used for convenience and all other work is done with infared light.

The second way of getting light onto a chip is via diffraction gratings, these are small structures which couple light into a waveguide, figure 3.2 shows this process from two views. Here the ideal coupling region is much larger, so there is no need for computer control and manual adjustment can suffice.

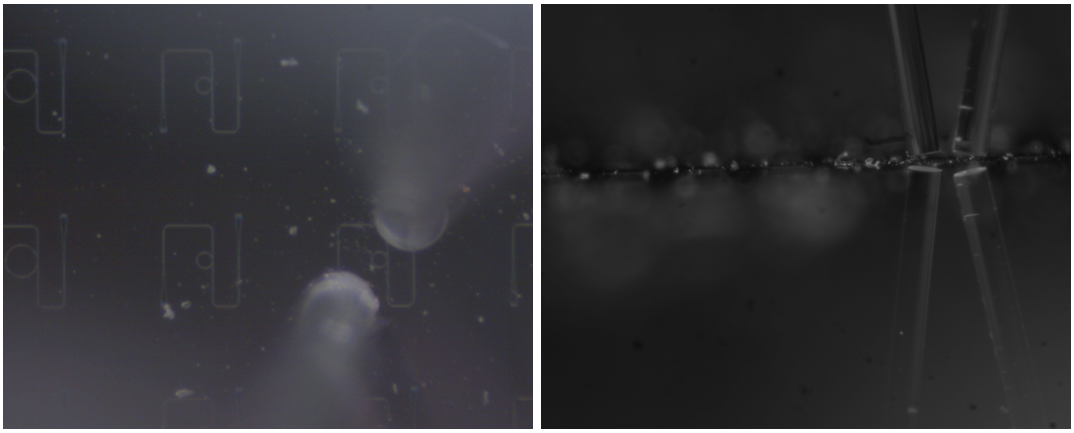

**Figure 3.2:** Side coupling proceedure

All of these coupling techniques rely on powermeters in the infrared region to maximise the transmission through the chip. Further the polarisation of the light must be adjusted to be inline with the mode which the devices is designed for.

With light reliably coupled into the chip a spectral scan of the wavelength range 1530 nm-1560 nm is typically performed to get a transmission spectra like in figure 2.6. With this the quality factor and the coupling coefficients of the particular ring can be calculated.

To begin the process for collecting a joint spectrum, the set up is arranged as in figure 3.3. This maintains the ability to do the above initial procedure. The two power meters allow the loss due to coupling to be monitored. This is typically on the order of 20 dB m.

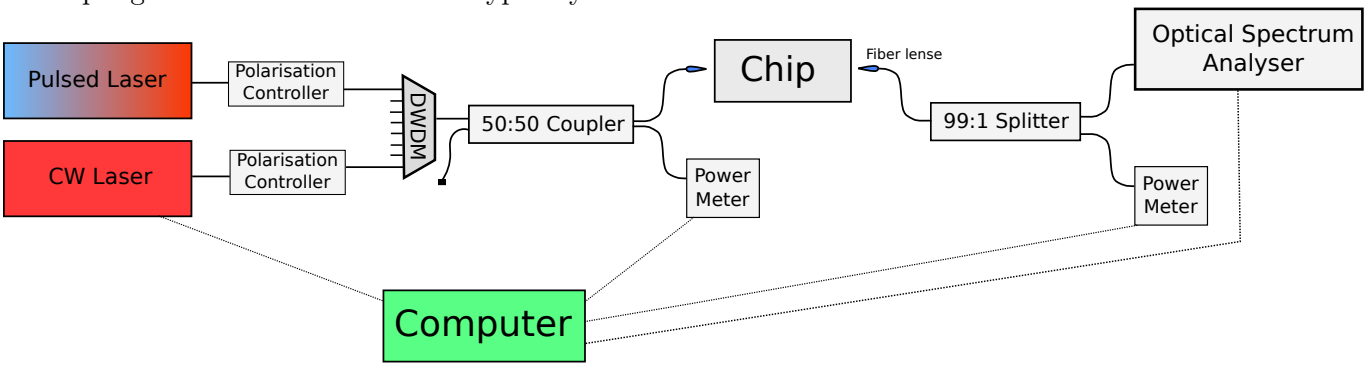


**Figure 3.3:** Glassgow test structure chip

The wavelength division multiplexer (DWDM) has 16 channels with 90 dB m noise suppression. These are used to suppress the amplified spontaneous emission (ASE) both lasers produce. With temperature control of the chip the resonances are tuned to the center of the DWDM channels. Then two resonances are chosen, onto one the pump is tuned and the other is connected to the CW laser in prepration for the stimulated four wave mixing.

Figure 3.4 is a key illustration of this experiment. One difference here is that the CW laser is instead filtered by a tunable filter as in figure 3.7 so the limits of the channel are not present. These are typically on the order of 1 nm.

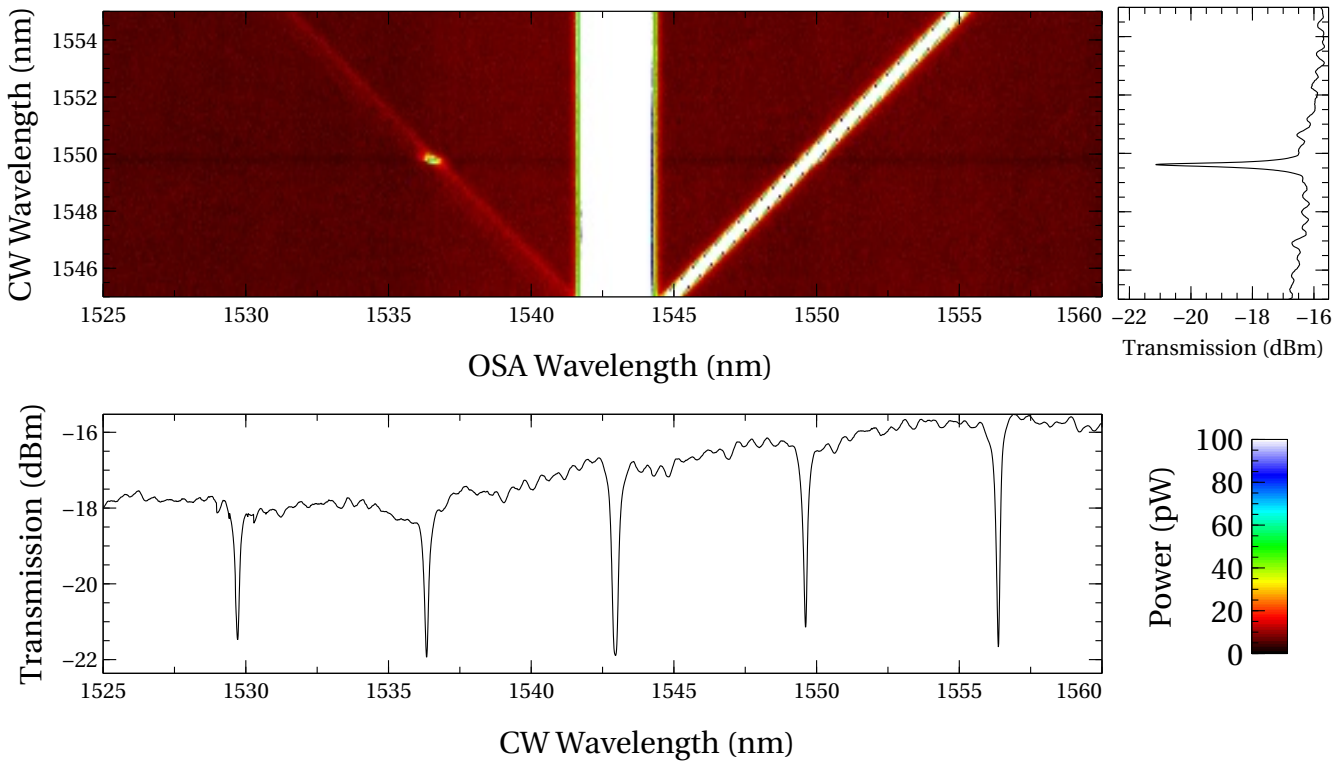


**Figure 3.4:** big picture

- **Glassgow**
- **Toshiba**
- **HP**

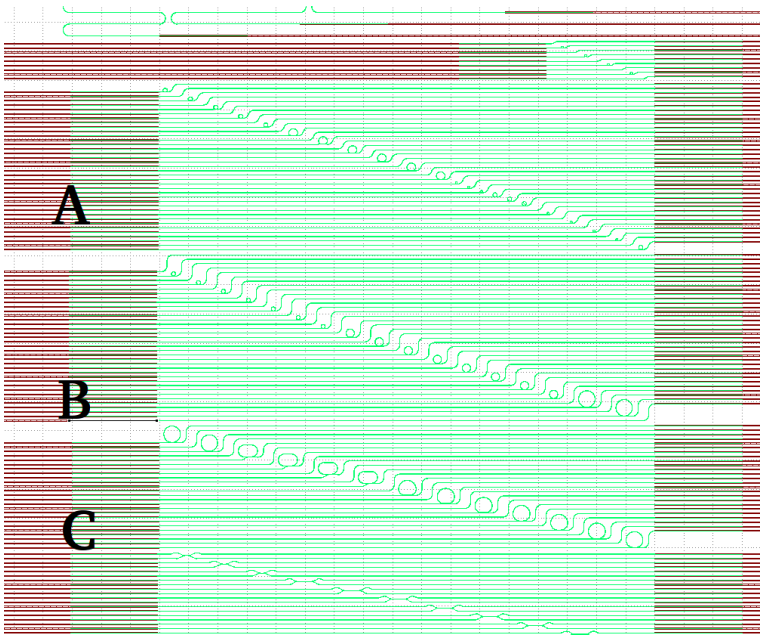


**Figure 3.5:** Glassgow test structure chip

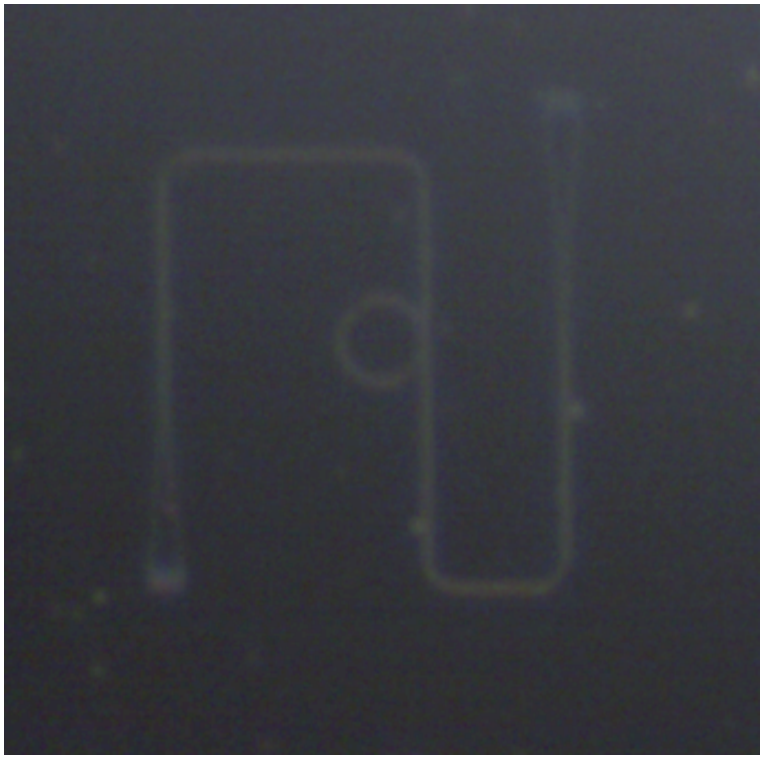

**Figure 3.6:** Glassgow test structure chip

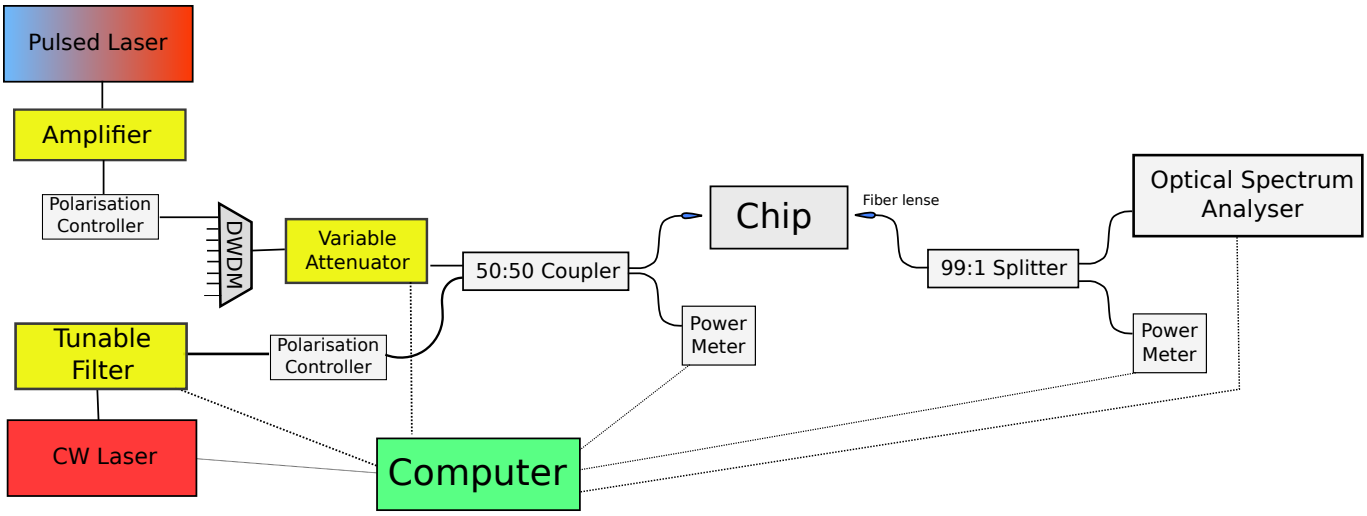


**Figure 3.7:** big experiment

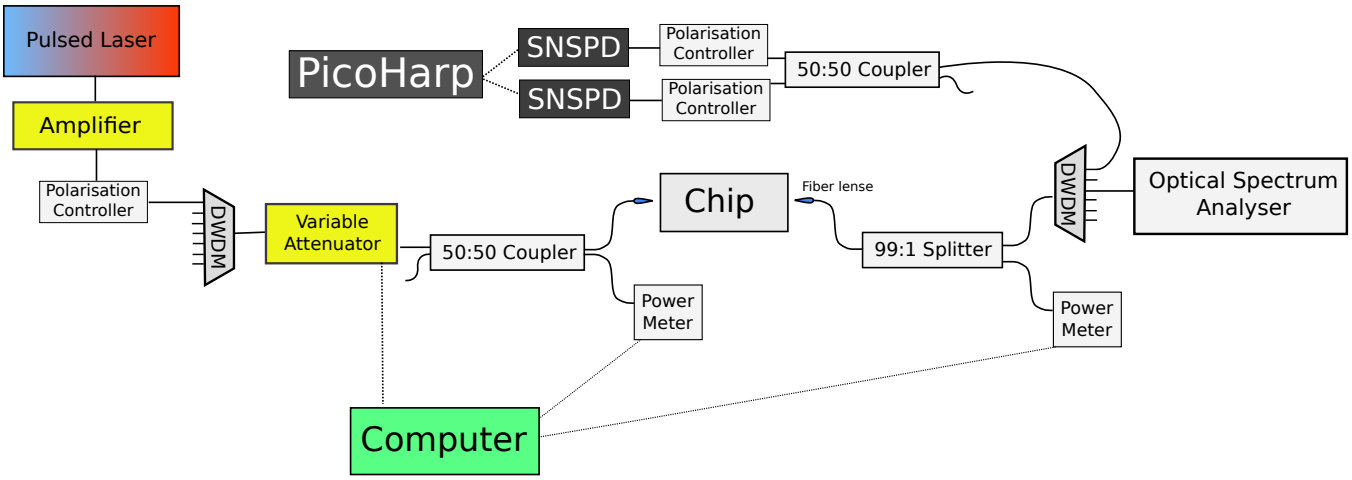


**Figure 3.8:** single photon

## 3.1 Joint Spectrum

Take the convention that the **signal** photon is the one we measure and the **idler** is the one we stimulate.

## 3.2 $g^{(2)}(0)$

## 3.3 Analysing Data

# 4 Results

## 4.1 Glassgow

This chip was used to do an initial proof of concept that the JSI of a ring resonator could be measured at high resolution. Here the aim was to explore different ring geometries and develop an intuition on how to do the experiment. The Pritel pulsed laser was used with a pulse duration of 2 ps, a FWHM of 1.0 nm with wavelength range 1530 nm to 1530 nm and a peak power of 100 W. Due to the pulsed laser sometimes destroying the spot size converter on the chip a 3 dB attenuator was added just after the laser output, this resulted in roughly about 5 dB m of power coming out of the lens fiber.

As each device on the chip has unique characteristics due to fabrication errors only some devices produced good data meaning that a full characterisation of the chip was not possible and only a few devices were used. Typically it was imperfections in the spot size converters on the chips being imperfect which prevented good JSI's from being collected but another issue encountered was under coupling of the rings.

Here we present three data sets collected, each has high SNR of at least 20 allowing for the maximum purity $P_{max}$ to be calculated with high accuracy. The relevant spectral scan is presented with the JSIs for reference, these are routine scans performed with the tunable CW laser typically at 1 m W of which roughly $-14$ dB m gets into the chip.

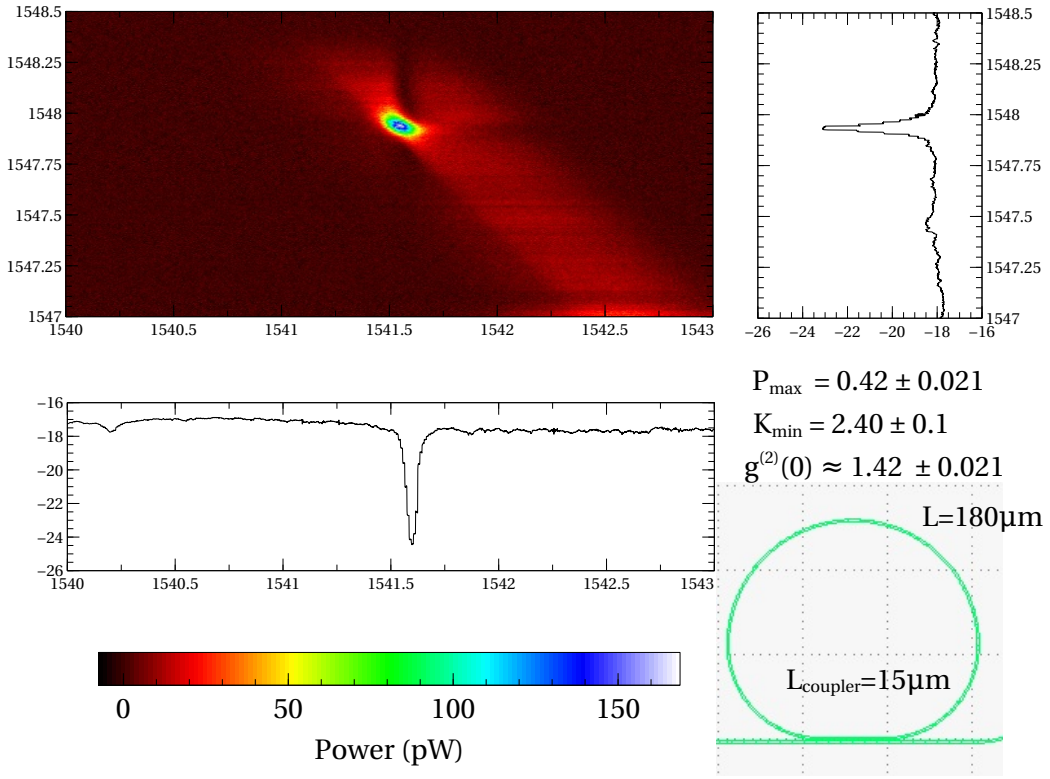

**Figure 4.1: JSI Ring C17** We calculate a quality factor of $Q \approx 25000$. In this instance the coupling loss was on average 20 dB and the input power of the pulsed laser was 5.1 dB giving a estimated power in waveguide of $-5$ dB. The probe laser operated at 1 m W. Fitting the spectral scans of the ring resonators gives coupling parameters of the order $r = 0.946$ $\tau = 0.985$ $n_{eff} = 4.136$, note these are only estimates.

Figure 4.1 shows a clear response from the ring resonator at the resonant frequencies, superimposed on this there is also straight waveguide stimulated four wave mixing observed at much lower intensities. It can be deduced that much of this straight wave guide contribution happens before the ring as it is filtered at the resonance wavelength. The asymmetry is an experimental artefact of imperfect alignment of the resonances with the AWG channels and the pump laser. This is $P_{max}$ value.

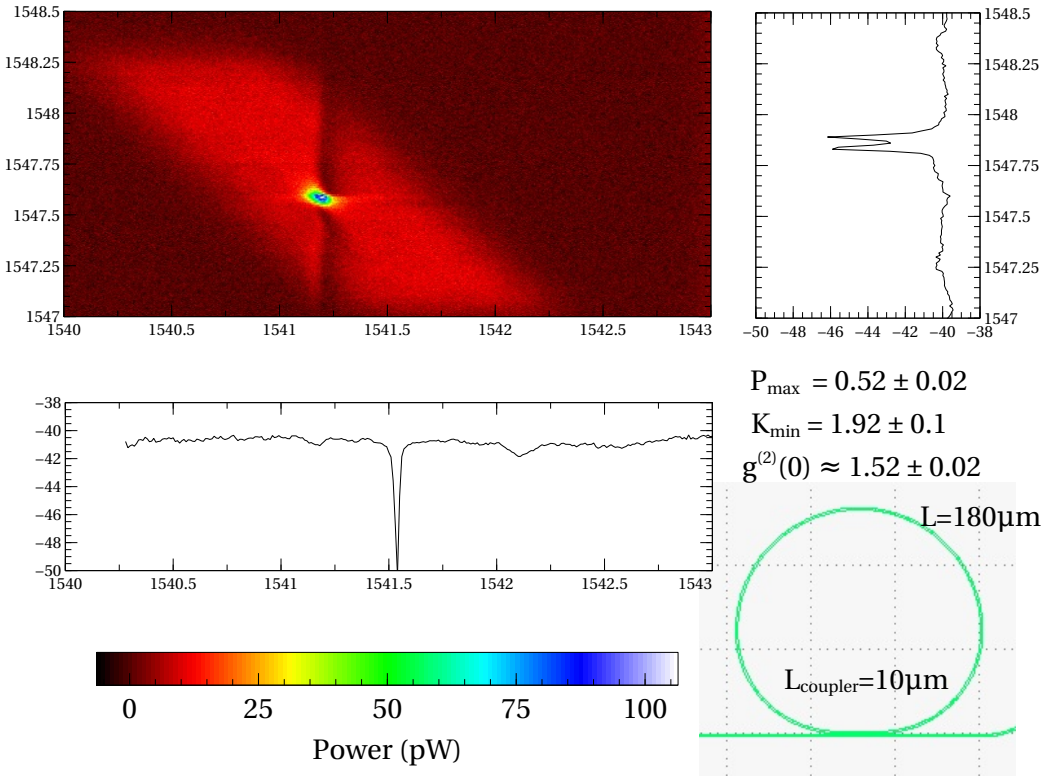


**Figure 4.2: JSI Ring C21** We calculate a quality factor of $Q \approx 28000$. In this instance the coupling loss was on average 21 dB and the input power of the pulsed laser was 5.5 dB m giving a estimated power in waveguide of $-5$ dB m. The probe laser operated at 1 m W. Fitting the spectral scans of the ring resonators gives coupling parameters of the order $r = 0.957$ $\tau = 0.977$ $n_{eff} = 4.144$, note these are only estimates.

In figure 4.2 we see ring C21 which has has many physical similarities with ring C17 shown in figure 4.1 however we observe a few key differences. Firstly the resonance that the CW laser probes is split but this is not reflected in the JSI because the split feature is on the order of 0.01 nm which under the 0.03 nm resolution of the OSA. This inability to resolve finer features which are almost certainly encoded in the real JSA is an important topic discussed later on in this work.

Secondly the coupling distance of the egg shaped resonator is slightly shorter here which is reflected in a slightly smaller value for $r$, however this difference isn't significant enough to use for a comparison as there are many other factors between the two experiments that were not held

constant, in particular the alignment of the AWG channels.

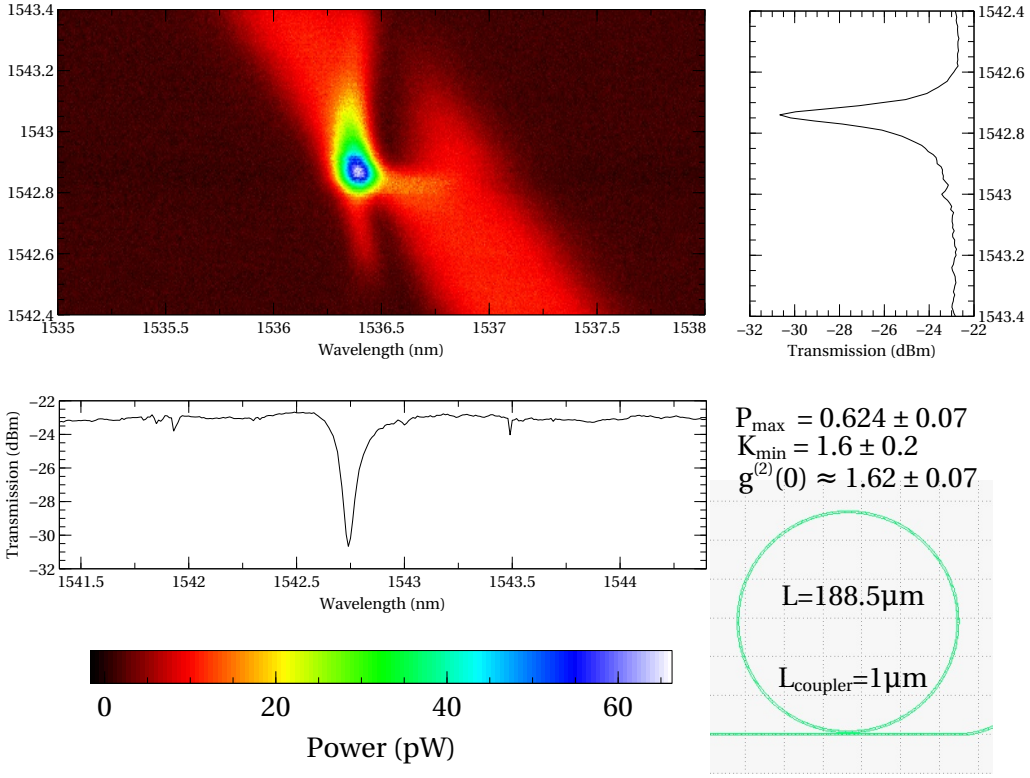


**Figure 4.3: JSI Ring B32** We calculate a quality factor of $Q \approx 14000$. In this instance the coupling loss was on average 22 dB m and the input power of the pulsed laser was 5.1 dB m giving a estimated power in waveguide of 0 dB m. The probe laser operated at 1 m W. Fitting the spectral scans of the ring resonators gives coupling parameters of the order $r = 0.985$ $\tau = 0.947$ $n_{eff} = 4.136$, note these are only estimates.

The final JSI collected for this chip is shown in figure 4.3, here the ring geometry is of the more traditional circular shape. It is observed that the resonance has some asymmetry due to more prominent non-linear effects. We observe the intensities of the ring resonator and straight wave guide FWM processes to be more similar in this scan which can be accounted for by the lower quality factory. Again it is notable to see that the ring seems to be collecting some of the straight wave guide FWM, however at a shifted frequency to the peak of the ring FWM, this is contradictory to the two previous examples and may be due to the more non-linear response of this ring.

**Summary** The three purities observed $(0.42, 0.52, 0.62)$ coincide with previous characterisations of the chip using the single photon detectors which measured a purity of on the order 0.45 [15]. A advantage to these measurements is they allow one to easier develop ways of increasing the purity.

## 4.2 a-Si

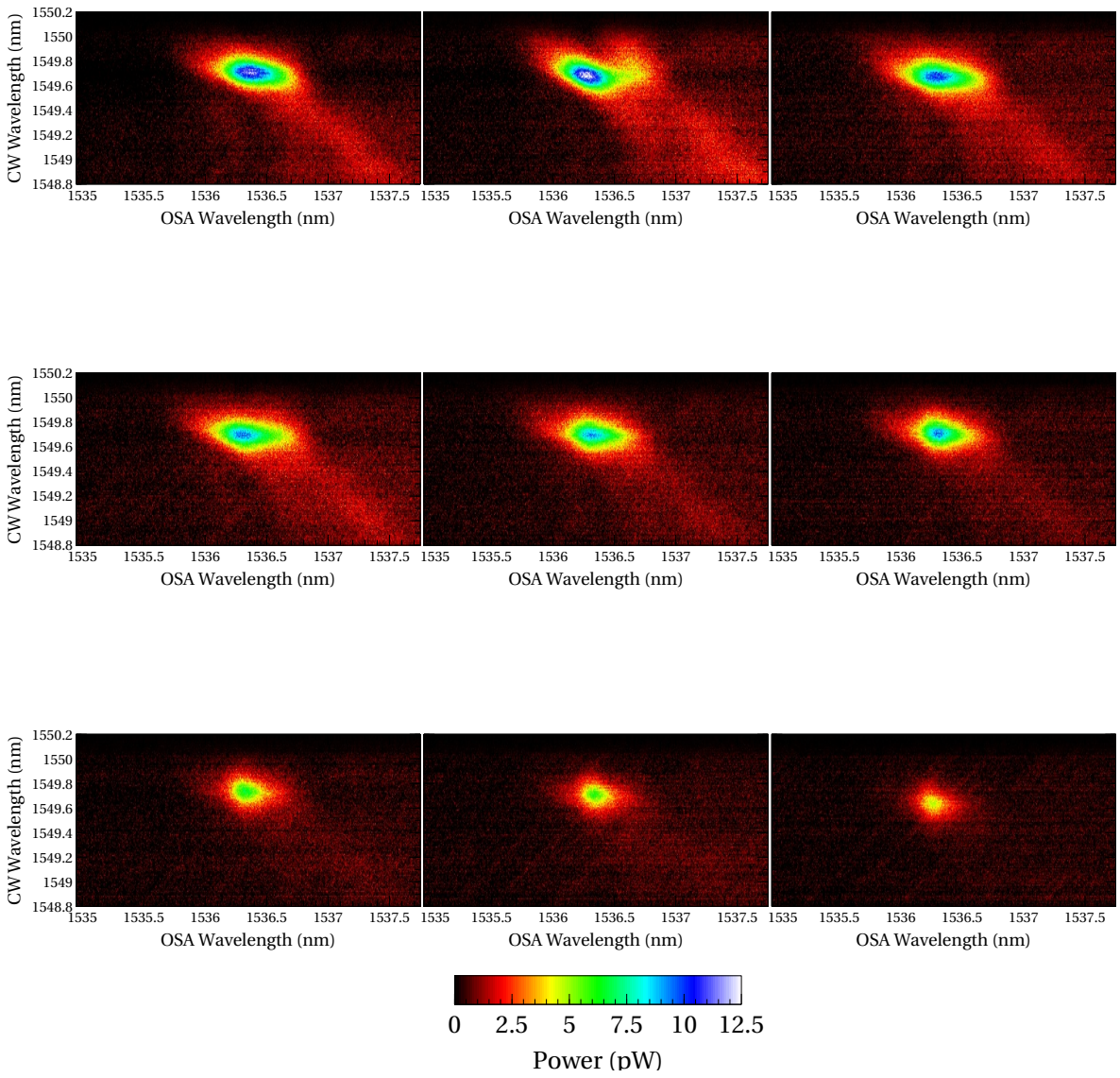


**Figure 4.4:** tit

# 5 Discussion

# 6 Conclusion

aueghuhgoehgosijegoisejgo

## References


[1] Richard P. Feynman. Simulating physics with computers. *Int J Theor Phys*, 21(6-7):467–488, June 1982.

[2] Peter W. Shor. Polynomial-Time Algorithms for Prime Factorization and Discrete Logarithms on a Quantum Computer. *arXiv:quant-ph/9508027*, August 1995. arXiv: quant-ph/9508027.

[3] Geza Toth and Iagoba Apellaniz. Quantum metrology from a quantum information science perspective. *Journal of Physics A: Mathematical and Theoretical*, 47(42):424006, October 2014. arXiv: 1405.4878.

[4] I.M. Georgescu, S. Ashhab, and Franco Nori. Quantum simulation. *Rev. Mod. Phys.*, 86(1):153–185, March 2014.

[5] P. Zhang, K. Aungskunsiri, E. Martn-Lpez, J. Wabnig, M. Lobino, R. W. Nock, J. Munns, D. Bonneau, P. Jiang, H. W. Li, A. Laing, J. G. Rarity, A. O. Niskanen, M. G. Thompson, and J. L. O'Brien. Reference-frame-independent quantum-key-distribution server with a telecom tether for an on-chip client. *Phys. Rev. Lett.*, 112(13):130501, April 2014.

[6] David P. DiVincenzo and Daniel Loss. Quantum Information is Physical. *Superlattices and Microstructures*, 23(3-4):419–432, March 1998. arXiv: cond-mat/9710259.

[7] Alfred B. URen, Yasser Jeronimo-Moreno, and Hipolito Garcia-Gracia. Generation of Fourier-transform-limited heralded single photons. *Phys. Rev. A*, 75(2):023810, February 2007.

[8] M. D. Eisaman, J. Fan, A. Migdall, and S. V. Polyakov. Invited Review Article: Single-photon sources and detectors. *Review of Scientific Instruments*, 82(7):071101, July 2011.

[9] J. W. Silverstone, D. Bonneau, K. Ohira, N. Suzuki, H. Yoshida, N. Iizuka, M. Ezaki, C. M. Natarajan, M. G. Tanner, R. H. Hadfield, V. Zwiller, G. D. Marshall, J. G. Rarity, J. L. O'Brien, and M. G. Thompson. On-chip quantum interference between silicon photon-pair sources. *Nat Photon*, 8(2):104–108, February 2014.

[10] Erman Engin, Damien Bonneau, Chandra M. Natarajan, Alex S. Clark, M. G. Tanner, R. H. Hadfield, Sanders N. Dorenbos, Val Zwiller, Kazuya Ohira, Nobuo Suzuki, Haruhiko Yoshida, Norio Iizuka, Mizunori Ezaki, Jeremy L. O?Brien, and Mark G. Thompson. Photon pair generation in a silicon micro-ring resonator with reverse bias enhancement. *Opt. Express*, 21(23):27826–27834, November 2013.

[11] Georg Harder, Vahid Ansari, Benjamin Brecht, Thomas Dirmeier, Christoph Marquardt, and Christine Silberhorn. An optimized photon pair source for quantum circuits. *Opt. Express*, 21(12):13975–13985, June 2013.

[12] Vilson R. Almeida and Michal Lipson. Optical bistability on a silicon chip. *Opt. Lett.*, 29(20):2387–2389, October 2004.

[13] Qianfan Xu and Michal Lipson. Carrier-induced optical bistability in silicon ring resonators. *Opt. Lett.*, 31(3):341–343, February 2006.

[14] Stefano Azzini, Davide Grassani, Matteo Galli, Lucio Claudio Andreani, Marc Sorel, Michael J. Strain, L. G. Helt, J. E. Sipe, Marco Liscidini, and Daniele Bajoni. From classical four-wave mixing to parametric fluorescence in silicon microring resonators. *Opt. Lett.*, 37(18):3807–3809, September 2012.

[15] Eric Scammell. Indistinguishable Heralded Photons from Silicon Ring Resonators, 2014.

# A Schmidt Number

## A.1 Definition

Starting with some abitrary state $\psi$:

$$|\psi\rangle = \sum_{i,j} \alpha(i,j)|i\rangle_A \otimes |j\rangle_B \tag{A.1}$$

The schimdt number $K$ of this state measures the degree of entanglement. If $K = 1$ then you can find $|\psi\rangle = |\xi\rangle \otimes |\eta\rangle$ and for $K > 1$ you can find:

$$|\psi\rangle = \sum_{i}^{K} r_i|\xi_i\rangle_A \otimes |\eta_i\rangle_B \tag{A.2}$$

Note that $1 \leq K \leq D$ where $D$ is the dimension of the system. The purity is the inverse of K so:

$$P = 1/K \tag{A.3}$$

An expression for $K$ can be found using the density matrix for $\psi$:

$$\rho_{AB} = |\psi\rangle\langle\psi| = \sum_{i,j,k,l} \alpha(i,j)\alpha^*(k,l)|i\rangle\langle k| \otimes |j\rangle\langle l| \tag{A.4}$$

$$\rho_A = \mathrm{Tr}_B(\rho_{AB}) = \sum_{i,j,k} \alpha(i,j)\alpha^*(k,j)|i\rangle\langle k| \tag{A.5}$$

$$\rho_A^2 = \sum_{i',j',k'} \sum_{i,j,k} \alpha(i,j)\alpha(k,j)\alpha^*(i',j')\alpha^*(k',j')|i\rangle\langle k|i'\rangle\langle k'| \tag{A.6}$$

$$= \sum_{j',k'} \sum_{i,j,k} \alpha(i,j)\alpha^*(k,j)\alpha(k,j')\alpha^*(k',j')|i\rangle\langle k'| \tag{A.7}$$

$$\mathrm{Tr}_A(\rho_A^2) = \sum_{i,j,k,j'} \alpha(i,j)\alpha^*(k,j)\alpha(k,j')\alpha^*(i,j') \tag{A.8}$$

$$\tag{A.9}$$

For a unentangled $\psi$ we know that $\mathrm{Tr}_A(\rho_A^2) = 1$ For $\psi$ entangled this will be smaller than 1 (proof comes from the property of the density operator that its eigenvalues are all smaller than 1). This fits the definiton of the purity of a quantum state hence we can write:

$$P = \frac{1}{K} = \sum_{i,j,k,l} \alpha(i,j)\alpha^*(k,j)\alpha(k,l)\alpha^*(i,l) \tag{A.10}$$

## A.2 Calculation from experimental data

### A.2.1 Trace method

In the lab we can measure $|\phi(\omega_1, \omega_2)|^2$, here I outline how to extract the schimdt number from this set of values. Taking the positive square root of the matrix of values obtained from the lab you have a matrix $\mathbf{f}$ given by:

$$\mathbf{f} = \sum_{\omega_1,\omega_2} \phi(\omega_1,\omega_2)|\omega_1\rangle\langle\omega_2| \tag{A.11}$$

(This seems to be some weird way of writing the wavefunction as a matrix, bare with me it turns out to be useful)

$$\mathbf{f}^\dagger\mathbf{f} = \sum_{\omega_1,\omega_2,\omega_3} \phi(\omega_1,\omega_2)\phi(\omega_3,\omega_2)|\omega_1\rangle\langle\omega_3| \tag{A.12}$$

$$(\mathbf{f}^\dagger\mathbf{f})^2 = \sum_{\omega_1,\omega_2,\omega_3,\omega_4,\omega_5,\omega_6} \phi(\omega_1,\omega_2)\phi(\omega_3,\omega_2)\phi(\omega_4,\omega_5)\phi(\omega_6,\omega_5)|\omega_1\rangle\langle\omega_3|\omega_4\rangle\langle\omega_6| \tag{A.13}$$

$$(\mathbf{f}^\dagger\mathbf{f})^2 = \sum_{\omega_1,\omega_2,\omega_3,\omega_4,\omega_5,\omega_6} \phi(\omega_1,\omega_2)\phi(\omega_3,\omega_2)\phi(\omega_3,\omega_5)\phi(\omega_6,\omega_5)|\omega_1\rangle\langle\omega_6| \tag{A.14}$$

$$\mathrm{Tr}\left[(\mathbf{f}^\dagger\mathbf{f})^2\right] = \sum_{\omega_1,\omega_2,\omega_3,\omega_4} \phi(\omega_1,\omega_2)\phi(\omega_3,\omega_2)\phi(\omega_3,\omega_4)\phi(\omega_1,\omega_4) \tag{A.15}$$

I've done it this way because I wanted to figure out where the equation in [**?**] comes from. You can now see that equation A.10 is of exactly the same form as $\mathrm{Tr}\left[(\mathbf{f}^\dagger\mathbf{f})^2\right]$ (barring the conjugates but this is okay since $\phi$ is real.) Taking the parallel further it can be seen that equation A.12 is of the form of a reduced density matrix. Here we must make sure to normalise to make sure this is a valid reduced density matrix. The normalisation is:

$$N = \mathrm{Tr}\left[\mathbf{f}^\dagger\mathbf{f}\right] = \sum_{\omega_1,\omega_2} \phi(\omega_1,\omega_2)^2 \tag{A.16}$$

Giving:

$$\rho_A = \frac{\mathbf{f}^\dagger\mathbf{f}}{N} \tag{A.17}$$

We can then write:

$$\frac{1}{K} = \frac{\mathrm{Tr}\left[(\mathbf{f}^\dagger\mathbf{f})^2\right]}{\mathrm{Tr}\left[\mathbf{f}^\dagger\mathbf{f}\right]^2} \tag{A.18}$$

### A.2.2 Alternate implementation with SVD decomposition

Taking the SVD decomposition of $\mathbf{f}$ gives:

$$\mathbf{f} = \sum_i |i\rangle s_i \langle i| \tag{A.19}$$

Where $s_i$ are the singular values. From wikipedia it turns out that $s_i^2$ are the eigenvalues of $\mathbf{f}^\dagger\mathbf{f}$ which is also equal to the reduced density operator. Following the steps of the previous section then gives:

$$\mathbf{f}^\dagger\mathbf{f} = \sum_i |i\rangle s_i^2 \langle i| \tag{A.20}$$

$$(\mathbf{f}^\dagger\mathbf{f})^2 = \sum_i |i\rangle s_i^4 \langle i| \tag{A.21}$$

And so:

$$\frac{1}{K} = \frac{\mathrm{Tr}\left[(\mathbf{f}^\dagger\mathbf{f})^2\right]}{\mathrm{Tr}\left[\mathbf{f}^\dagger\mathbf{f}\right]^2} = \frac{\sum_i s_i^4}{\left(\sum_j s_j^2\right)^2} = \sum_i \left(\frac{s_i^2}{\sum_j s_j^2}\right)^2 \tag{A.22}$$

# B Equipment Specifications

# C Transfer matrix analysis of ring resonator cavities

A useful way to describe the spectral response of a ring resonator is by defining a transfer matrix. This $2\times2$ matrix relates the electric fields of the inputs and outputs of the waveguide and resonator. In our analysis we define the electric fields to be complex valued and also normalised to conserve energy, this condition implies the transfer matrix must be unitary.

First write down the obvious relations

$$E_{out} = r_1 E_{in} + t_1 E_2 \tag{C.1}$$

$$E_1 = r_2 E_2 + t_2 E_{in} \tag{C.2}$$

Define a matrix.

$$M = \begin{pmatrix} r_1 & t_1 \\ t_2 & r_2 \end{pmatrix} \tag{C.3}$$

Enforce unitarity

$$\begin{pmatrix} r_1 & t_1 \\ t_2 & r_2 \end{pmatrix} \begin{pmatrix} r_1^* & t_2^* \\ t_1^* & r_2^* \end{pmatrix} = \begin{pmatrix} |r_1|^2 + |t_1|^2 & r_1 t_2^* + r_2^* t_1 \\ r_2 t_1^* + r_1^* t_2 & |r_2|^2 + |t_2|^2 \end{pmatrix} = \begin{pmatrix} 1 & 0 \\ 0 & 1 \end{pmatrix} \tag{C.4}$$

Furthermore $\det M = 1$

$$r_1 r_2 - t_1 t_2 = 1 \tag{C.5}$$

so

$$r_2 = \frac{1 + t_1 t_2}{r_1} \tag{C.6}$$

Also $M^{-1} = M^*$

$$\begin{pmatrix} r_2 & -t_1 \\ -t_2 & r_1 \end{pmatrix} = \begin{pmatrix} r_1^* & t_1^* \\ t_2^* & r_2^* \end{pmatrix} \tag{C.7}$$

This tells us $r_1$ and $r_2$ must be real. So we can simplify the unitarity equation. So

$$t_1 = iT_1 \tag{C.8}$$

$$t_2 = iT_2 \tag{C.9}$$

Rewrite the interesting equations: Use also $r_2 = r_1^*$

$$\begin{pmatrix} |r_1|^2 + T_1^2 & -ir_1 T_2 + ir_1 T_1 \\ -ir_1^* T_1 + ir_1^* T_2 & |r_1|^2 + T_2^2 \end{pmatrix} = \begin{pmatrix} 1 & 0 \\ 0 & 1 \end{pmatrix} \tag{C.10}$$

Ok so $T_2 = T_1 = t$

$$\begin{pmatrix} |r_1|^2 + t^2 & 0 \\ 0 & |r_1|^2 + t^2 \end{pmatrix} = \begin{pmatrix} 1 & 0 \\ 0 & 1 \end{pmatrix} \tag{C.11}$$

$$|r_1|^2 = 1 - t^2 \tag{C.12}$$

$$|r_2|^2 = 1 - t^2 \tag{C.13}$$

d Basically I have a degree of freedom. $r_1 = e^{i\theta}r$ and $r_2 = e^{-i\theta}r$. Choose $\theta = 0$ for simplicity.

Now the matrix is:

$$\begin{pmatrix} r & it \\ it & r \end{pmatrix} \tag{C.14}$$

Now we add that

$$E_2 = \tau e^{i\theta} E_1$$

Recall the initial equations.

$$E_{out} = rE_{in} + itE_2 \tag{C.15}$$

$$E_1 = rE_2 + itE_{in} \tag{C.16}$$

$$E_1 = r\tau e^{i\theta} E_1 + itE_{in} \tag{C.17}$$

$$\frac{E_1}{E_0} = \frac{it}{1 - r\tau e^{i\theta}} \tag{C.18}$$

Okay so thats $E_1$ done.

$$\frac{E_1}{E_0} = \frac{it}{1 - r\tau e^{i\theta}} \tag{C.19}$$

$$\left|\frac{E_1}{E_0}\right|^2 = \frac{t^2}{1 + r^2\tau^2 - 2r\tau cos(\theta)} \tag{C.20}$$

For $E_2$ we have:

$$\frac{E_2}{E_0} = \frac{it\tau e^{i\theta}}{1 - r\tau e^{i\theta}} \tag{C.21}$$

$$\left|\frac{E_2}{E_0}\right|^2 = \frac{\tau^2 - \tau^2 r^2}{1 + r^2\tau^2 - 2r\tau cos(\theta)} \tag{C.22}$$

For $E_{out}$ we have:

$$\frac{E_{out}}{E_0} = r + it\frac{it\tau e^{i\theta}}{1 - r\tau e^{i\theta}} \tag{C.23}$$

$$\frac{E_{out}}{E_0} = \frac{r - r^2\tau e^{i\theta} - t^2\tau e^{i\theta}}{1 - r\tau e^{i\theta}} \tag{C.24}$$

$$\left|\frac{E_{out}}{E_0}\right|^2 = \frac{(r - r^2\tau e^{i\theta} - t^2\tau e^{i\theta})(r - r^2\tau e^{-i\theta} - t^2\tau e^{-i\theta})}{(1 - r\tau e^{i\theta})(1 - r\tau e^{-i\theta})} \tag{C.25}$$

$$\left|\frac{E_{out}}{E_0}\right|^2 = \frac{(r(r - r^2\tau e^{-i\theta} - t^2\tau e^{-i\theta}) - r^2\tau e^{i\theta}(r - r^2\tau e^{-i\theta} - t^2\tau e^{-i\theta}) - t^2\tau e^{i\theta}(r - r^2\tau e^{-i\theta} - t^2\tau e^{-i\theta}))}{1 + r^2\tau^2 - 2r\tau cos(\theta)} \tag{C.26}$$

$$\left|\frac{E_{out}}{E_0}\right|^2 = \frac{r^2 - r^3\tau e^{-i\theta} - rt^2\tau e^{-i\theta} - r^3\tau e^{i\theta} + r^4\tau^2 + 2r^2\tau^2 t^2 - rt^2\tau e^{i\theta} + t^4\tau^2}{1 + r^2\tau^2 - 2r\tau cos(\theta)} \tag{C.27}$$

$$\left|\frac{E_{out}}{E_0}\right|^2 = \frac{r^2 - e^{-i\theta}(r^3\tau + rt^2\tau) - e^{i\theta}(r^3\tau + rt^2\tau) + r^4\tau^2 + t^4\tau^2 + 2r^2\tau^2 t^2}{1 + r^2\tau^2 - 2r\tau cos(\theta)} \tag{C.28}$$

$$\left|\frac{E_{out}}{E_0}\right|^2 = \frac{r^2 + 2(r^3\tau + rt^2\tau)\cos(\theta) + r^4\tau^2 + t^4\tau^2 + 2r^2\tau^2 t^2}{1 + r^2\tau^2 - 2r\tau cos(\theta)} \tag{C.29}$$

$$\left|\frac{E_{out}}{E_0}\right|^2 = \frac{r^2 2(r^3\tau + r(1-r^2)\tau)\cos(\theta) + r^4\tau^2 + (1-r^2)^2\tau^2 + 2r^2\tau^2(1-r^2)}{1 + r^2\tau^2 - 2r\tau cos(\theta)} \tag{C.30}$$

$$\left|\frac{E_{out}}{E_0}\right|^2 = \frac{r^2 - 2(r^3\tau + r(1-r^2)\tau)\cos(\theta) + r^4\tau^2 + (1-2r^2+r^4)\tau^2 + 2r^2\tau^2 - 2r^4\tau^2}{1 + r^2\tau^2 - 2r\tau cos(\theta)} \tag{C.31}$$

$$\left|\frac{E_{out}}{E_0}\right|^2 = \frac{r^2 - 2r\tau\cos(\theta) + r^4\tau^2 + \tau^2 - 2r^2\tau^2 + r^4\tau^2 + 2r^2\tau^2 - 2r^4\tau^2}{1 + r^2\tau^2 - 2r\tau cos(\theta)} \tag{C.32}$$

**FINAL RESULTS**

$$\left|\frac{E_{out}}{E_0}\right|^2 = \frac{r^2 - 2r\tau\cos(\theta) + \tau^2}{1 + r^2\tau^2 - 2r\tau cos(\theta)} \tag{C.33}$$

$$\left|\frac{E_2}{E_0}\right|^2 = \frac{\tau^2 - \tau^2 r^2}{1 + r^2\tau^2 - 2r\tau cos(\theta)} = \tau^2 \left|\frac{E_1}{E_0}\right|^2 \tag{C.34}$$

$$\left|\frac{E_1}{E_0}\right|^2 = \frac{t^2}{1 + r^2\tau^2 - 2r\tau cos(\theta)} \tag{C.35}$$